Journal of Analytical and Applied Pyrolysis xxx (xxxx) xxx–xxx

Contents lists available at ScienceDirect

Journal of Analytical and Applied Pyrolysis

journal homepage: www.elsevier.com/locate/jaap

Catalytic mechanism of sulfuric acid in cellulose pyrolysis: A combined experimental and computational investigation

Bin Hu, Qiang Lu*, Yu-ting Wu, Zhen-xi Zhang, Min-shu Cui, Ding-jia Liu, Chang-qing Dong, Yong-ping Yang

National Engineering Laboratory for Biomass Power Generation Equipment, North China Electric Power University, Beijing, 102206, China

ARTICLE INFO

Keywords:
Cellulose pyrolysis
Sulfuric acid
Catalytic mechanism
DFT
TGA
Py-GC/MS

ABSTRACT

Sulfuric acid (H_2SO_4) is widely used as a strong acid catalyst in biomass pyrolysis process, and exhibits prominent catalytic effects on the pyrolytic reactions and product distribution. In this study, the fundamental catalytic mechanism of H_2SO_4 on cellulose pyrolysis process was investigated via combined experimental and computational methods. Both thermographic analysis (TGA) and pyrolysis–gas chromatography/mass spectrometry (Py–GC/MS) experiments were performed to reveal the pyrolytic characteristics and product distribution in the H_2SO_4-catalyzed pyrolysis of cellulose. In addition, quantum chemistry methods were employed to build the reaction models and investigate the major H_2SO_4-assisted reactions in initial cellulose pyrolysis process, i.e., depolymerization of the cellulose chain, bridged dehydration, ring-opening, ring-contraction and dehydration of the free hydroxyl groups. The results indicate that the H_2SO_4-assisted depolymerization via C1-O1 bond scission and bridged dehydration reactions take place in a two-step mechanism involving a sulfate ester intermediate. While other reactions occur via a one-step mechanism involving only hydroxyl group or both hydroxyl and sulfonic groups of H_2SO_4. The activation energies of above reactions are all decreased by adding H_2SO_4, and thus lowering the degradation temperature of cellulose. Among all initial pyrolytic reactions, dehydration reactions which are inconspicuous in the non-catalytic process, become very important in the catalytic process, because their activation energies are decreased dramatically by adding H_2SO_4 (from 322.7 to 372.1 to 152.2–237.7 kJ/mol). The promoting effect on the dehydration reactions plays a vital role in the increased char yield and significant change of organic volatile product distribution. Through the promoted dehydration reactions, unsaturated structures of cellulose are formed, which is favorable for the formation of certain dehydrated products at the expense of depolymerized and ring scission products.

1. Introduction

Conventional fast pyrolysis of biomass is a non-selective thermal conversion process to obtain a very complex liquid product known as bio-oil. The complex chemical composition and poor properties of crude bio-oil significantly limit its utilization in current industries [1]. In order to solve this problem, catalytic pyrolysis has been proposed as a promising way to selectively control the biomass pyrolysis process towards specific bio-oils [2,3]. Inorganic acids have been widely utilized to catalyze the biomass pyrolysis process, including H_2SO_4 [4,5], phosphoric acid (H_3PO_4) [6,7] and nitric acid (HNO_3) [8]. These acid catalysts are very effective to significantly alter the biomass pyrolysis characteristics as well as product distribution, and can be utilized to prepare value-added chemicals [7,8].

H_2SO_4 is a common strong inorganic acid, and has been widely employed for catalytic pyrolysis of biomass and its primary components (cellulose, hemicellulose and lignin). The catalytic effect of H_2SO_4 on cellulose pyrolysis has been preliminarily elucidated as summarized by the following three aspects. Firstly, the initial decomposition temperature of cellulose will be significantly decreased by H_2SO_4. This fact has been confirmed by previous work [7–10] according to TGA studies on the H_2SO_4 impregnated cellulose. Secondly, the promoting effect of H_2SO_4 on dehydration and charring reactions changes the yields of solid, liquid and gas products. Char and water yields increase, while that of organic liquid compounds (organic fraction of bio-oil) decreases. Such catalytic effects will be promoted along with the increase of H_2SO_4 content [8–11]. Thirdly, pyrolytic product composition will also be altered by H_2SO_4. In regard to the liquid products, H_2SO_4 can significantly decrease the yield of levoglucosan (LG) which is the typical depolymerized product and also the most abundant pyrolytic product in

* Corresponding author.
E-mail addresses: qianglu@mail.ustc.edu.cn, qlu@ncepu.edu.cn (Q. Lu).

https://doi.org/10.1016/j.jaap.2018.06.007
Received 7 April 2018; Received in revised form 28 May 2018; Accepted 4 June 2018

bio-oil. Meanwhile, yields of several dehydrated products can be increased, such as 1,4:3,6-dianhydro-α-D-glucopyranose (DGP), furfural (FF) and levoglucosenone (LGO). Detailed H_2SO_4-catalyzed product distribution generally differed in previous studies due to different impregnation methods, pyrolytic conditions and H_2SO_4 contents [7]. However, the basic conclusions were not controversial based on the fact that H_2SO_4 could promote dehydration and cross-linking reactions [12].

Currently, the published studies on H_2SO_4-catalyzed pyrolysis of cellulose mainly paid attention to the catalytic behaviors of H_2SO_4, neglecting deep insight into the catalytic mechanism. In regard to the catalytic center of H_2SO_4 (proton or acid ion), different viewpoints were raised. Nimlos et al. [13,14] proposed the proton-catalyzed mechanism for ethanol pyrolytic reactions based on the quantum chemistry calculation. It was found that protonated ethanol/carbohydrates would readily undergo dehydration reactions with relatively low activation energies. On the contrary, Julien et al. [8] regarded that the pyrolysis reactions were mainly catalyzed by the sulfate ion. In comparison of catalytic pyrolysis of cellulose over different inorganic acids [4–8], both similarities and distinctions exist, indicating that both the proton and the acid ion should play vital roles in influencing the pyrolytic reactions of cellulose. In addition, the stability of ions is questionable under a fluent gas condition in the pyrolysis process, especially the carrier gases (usually N_2 and He) having low dielectric constants [15]. Therefore, it is necessary to consider the global effect of the acid molecule on the cellulose pyrolysis.

In the present study, catalytic effect of H_2SO_4 on cellulose pyrolysis was investigated in detail using computational chemistry methods. Three model compounds, i.e.,1,4-dimethyl-glucose, 4-methyl-glucose and 1-methyl-glucose were selected to investigate the effect of H_2SO_4 on major cellulose initial decomposition reactions, i.e., depolymerization of cellulose chain, bridged dehydration, ring-opening, ring-contraction and dehydration of the free hydroxyl groups, as shown in Fig. 1. Structural analyses and kinetic analyses were conducted based on the computational results. Meanwhile, TGA and Py-GC/MS experiments were performed to combine with the computational investigation to give an insight into the catalytic mechanism of H_2SO_4 on cellulose pyrolysis.

2. Methods

2.1. Experimental section

2.1.1. Materials

Microcrystalline cellulose (Avicel PH-101, Sigma) was employed for the pyrolysis experiments. H_2SO_4 impregnated cellulose was prepared by the incipient wetness impregnation method [16]. H_2SO_4 solutions with different concentrations were prepared by adding concentrated H_2SO_4 (AR, 98%) to different volumes of deionized water. Then 1 g cellulose was added to 3 ml diluted H_2SO_4 solution to obtain a gel-like paste. The mixture was treated in the KQ-500DE ultrasonic sonicator (Kunshan Utranonis Istrument, CO., LTD, 40 kHz) for 7 h. Then the sample was dried (35 °C in air for 2 h) and ground to obtain fine powders. The sample was stored in a desiccator for experiments. A total of six samples were prepared with the H_2SO_4 contents of 0 wt%, 1.0 wt %, 3.0 wt%, 5.0 wt%, 10.0 wt% and 20.0 wt%, respectively.

2.1.2. TGA analysis

TGA experiments of the H_2SO_4 impregnated cellulose samples were performed on an STA600 thermogravimetric analyzer (Perkin Elmer). The samples (10 mg) were heated from room temperature to 900 °C at a heating rate of 20 °C/min under nitrogen gas (20 mL/min).

2.1.3. Py-GC/MS Experiments

Fast pyrolysis experiments were conducted by using the CDS Pyroprobe 5200HP pyrolyzer (Chemical Data Systems) connected with a Perkin Elmer GC/MS (Clarus 560). The experimental samples were prepared by filling the cellulose sample in the middle of the quartz tube, and quartz wool was placed at both ends to hold the sample. In each sample, the quantity of the H_2SO_4 impregnated cellulose varied to ensure the pure cellulose quantity of 0.20 mg. As a result, the actual quantities of the pretreated cellulose samples were precisely weighed to be 0.20 mg, 0.20 mg, 0.21 mg, 0.21 mg, 0.22 mg and 0.25 mg, corresponding to H_2SO_4 contents of 0 wt%, 1.0 wt%, 3.0 wt%, 5.0 wt%, 10.0 wt% and 20.0 wt%, respectively. An analytical balance (XS105, METTLER TOLEDO) with a readability of ± 0.01 mg was used for weighing.

Pyrolysis was performed under 500 °C for 20 s with a heating rate of 20 °C/ms. The pyrolysis vapor went into GC/MS for analysis with carrier gas (helium, 99.999%, 1 mL/min). GC separation was achieved by an Elite-35MS capillary column (30 m × 0.25 mm i.d., 0.25 μm of film thickness) with a split ratio of 1:80. The GC oven was heated from 40 °C to 280 °C at a heating rate of 15 °C/min, then was held at 280 °C for 2 min. The GC/MS interface was held at 280 °C. The mass spectrometer was operated in electron ionization (EI) mode at 70 eV. The chromatographic peaks were identified according to NIST library, Wiley library and the literature data. For each sample, the experiments were replicated for at least three times to confirm the reproducibility of the reported results.

2.2. Computational section

2.2.1. Computational methods

Gaussian 09 package [17] was used for all density functional theory

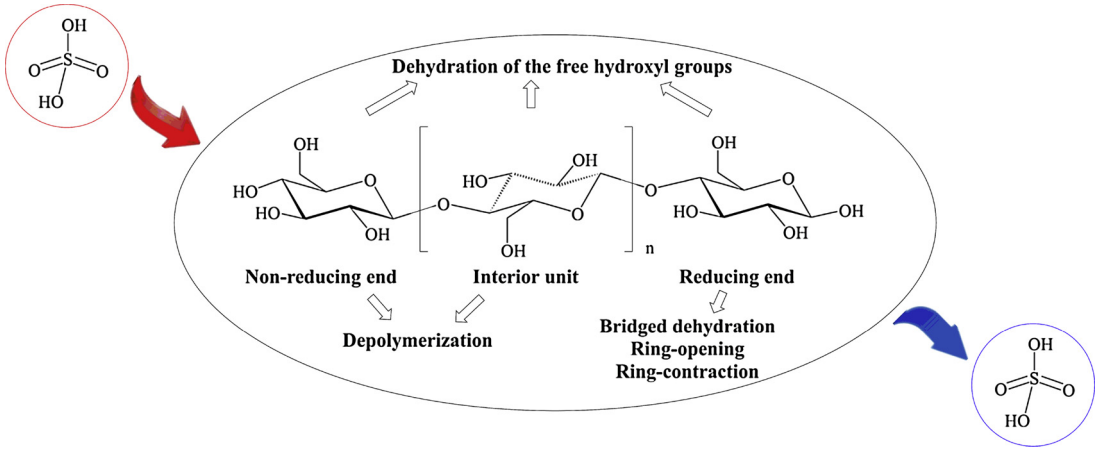

Fig. 1. Major H_2SO_4-catalyzed pyrolytic reactions in initial cellulose pyrolysis process.

(DFT) [18,19] calculations. The structures of all the compounds were optimized by using B3LYP-D3 method and 6–311 g(d,p) basis set. "D3" is one of the dispersion correction methods for DFT calculation which can improve the accuracy of hydrogen bonds or p-π interaction description [20]. Frequency analyses [21] of the optimized structures were conducted at the same level. The one and only imaginary frequency of every transition state and no imaginary frequency for other compounds confirmed the validity of the calculation. Afterwards, intrinsic reaction coordinate (IRC) [22] analyses were performed to verify if the transition states were the first-order saddle points on the potential energy surfaces. The variations of the Mayer bond orders along with IRC coordinates were analyzed by using Multiwfn software [23]. Furthermore, single point energies were calculated at M06-2X-D3/def2TZVP level for all compounds optimized at B3LYP-D3/6–311 g(d,p) level to obtain a more accurate estimate of the energy barriers.

Kinetic analyses were conducted based on the DFT calculation results by using KiSTheIP software [24]. Rate constants (k) were calculated based on transition state theory (TST) [25] with Wigner tunneling correction [26] for elementary reactions. Activation energy (E_a) and pre-exponential factor (A) were estimated based on Arrhenius equation of $k = A\mathrm{EXP}(-E_a/\mathrm{RT})$.

2.2.2. Computational model

Cellulose is a linear homopolysaccharide of glucose units linked by the β-1,4-glucosidic bond. As shown in Fig. 2, cellulose has three characteristic units, i.e., interior unit, reducing end and non-reducing end. In order to fully understand the cellulose pyrolysis process, 1,4-dimethyl-glucose (model compound 1, **MC1**), 4-methyl-glucose (model compound 2, **MC2**) and 1-methyl-glucose (model compound 3, **MC3**) are selected to represent the three characteristic units, respectively. For the three model compounds, the methoxyl groups linked to C1 and/or C4 position were adopted to simulate the glucosidic bonds. Similar methods were also adopted in previous literatures [27,28]. Fig. 2 also shows the molecular geometries of **MC1**, **MC2**, **MC3** and H_2SO_4 with all the atoms being numbered conventionally. Nishiyama et al. [29] reported that the hydroxymethyl group at C6 position was in *tg* conformation. Hence the *tg* conformation was adopted for all the model compounds. In regard to H_2SO_4, the reactivity of the two S—O bonds are the same due to the structural symmetry, so are the two S=O bonds. Detailed structures and atomic coordinates of the model compounds and all the structures involved in the pyrolytic reactions are shown in the Supplementary Material (*Section S6*).

3. Results and discussion

3.1. Experimental results

3.1.1. TGA results

Fig. 3 shows the thermogravimetry (TG) and differential thermogravimetry (DTG) curves of cellulose samples with different H_2SO_4 contents. The weight loss below 100 °C was attributed to the evaporation of imbibed water [30]. For pure cellulose, the onset temperature of degradation (T_{onset}) and the temperature of maximum weight loss rate (T_{max}) were 300 °C and 348 °C respectively, which were close to the literature results [9,10,30]. When H_2SO_4 was impregnated on the cellulose, both T_{onset} and T_{max} shifted to the low temperature region (120–180 °C for T_{onset}, 150–235 °C for T_{max}). The decrease of T_{onset} and T_{max} was enhanced along with the increasing of H_2SO_4 content. Another weight loss region (300–550 °C) emerged for the H_2SO_4 impregnated cellulose, which could be attributed to the decomposition of H_2SO_4 into water and sulfur dioxide/trioxide at elevated temperatures [10]. The presence of H_2SO_4 greatly increased the char yield. According to the TG curves, the mass of the residue increased monotonously along with rising H_2SO_4 content to 5 wt%. A slight decrease was then observed at higher H_2SO_4 contents, which was also reported by Kang et al. [9]. The decrease of the residue mass at higher H_2SO_4 contents should be ascribed to the decomposition of H_2SO_4 at elevated temperatures [10]. Previous studies have confirmed that the residue from H_2SO_4 impregnated cellulose is nearly pure carbon with only trace sulfur [10]. Therefore, the actual char yields from pretreated cellulose samples could be calculated based on the residue yields and H_2SO_4 contents in cellulose. The calculation results indicated that the actual char yields were 7.5 wt%, 20.5 wt%, 24.5 wt%, 26.9 wt%, 28.1 wt% and 31.1 wt%, corresponding to H_2SO_4 contents of 0 wt%, 1.0 wt%, 3.0 wt%, 5.0 wt%, 10.0 wt% and 20.0 wt%, respectively. These data were similar to the char yields reported by Kang and co-workers [9].

3.1.2. Py-GC/MS Results

Typical total ion chromatograms from non-catalytic and H_2SO_4-catalyzed pyrolysis of cellulose are given in Fig. 4. The pyrolytic product distribution from non-catalytic pyrolysis of cellulose agreed with previous results [31,32], including various anhydrosugars (LG, LGO, LAC, DGP, APP, AGF, etc.), linear carbonyls (HAA, HA, etc.), furans (5-HMF, FF, etc.), and so on. LG (peak 10) is the typical depolymerized product of cellulose [33,34], and it is also the most abundant pyrolytic product. HAA (peak 1, the second most abundant product) and HA (peak 3) are the typical ring scission products [33,35]. FF (peak 4), LGO (peak 5), LAC (peak 6), DGP (peak 7) and APP (peak 9) are the typical

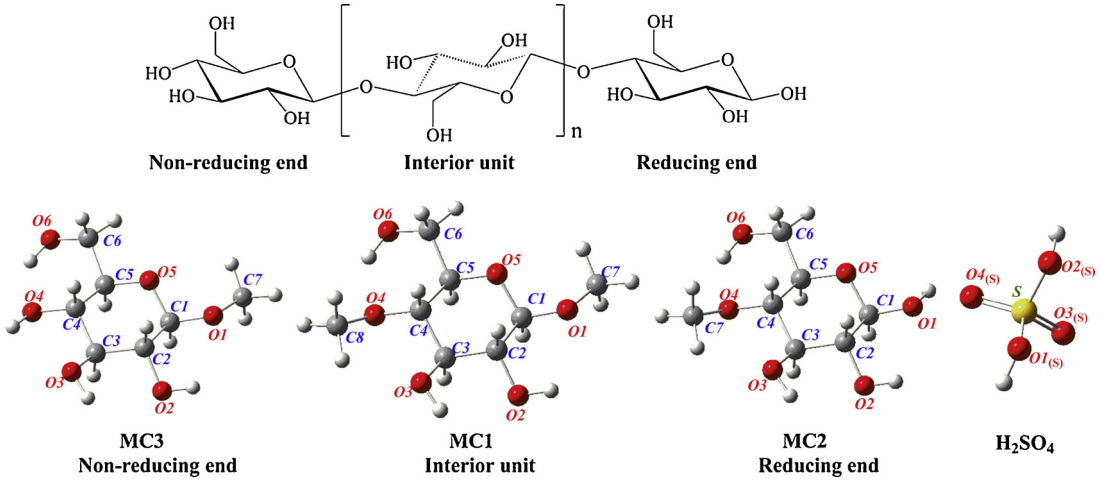

Fig. 2. Structures of **MC1**, **MC2**, **MC3** and H_2SO_4.

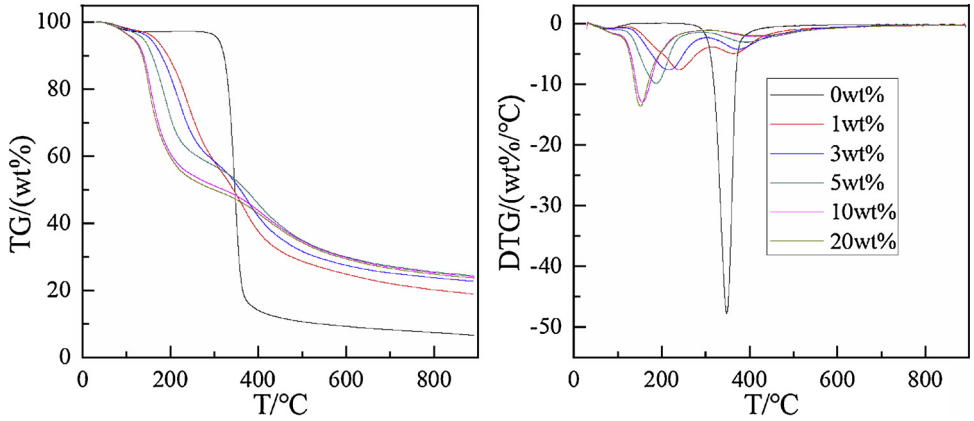

Fig. 3. TG and DTG curves of cellulose samples with different H_2SO_4 contents.

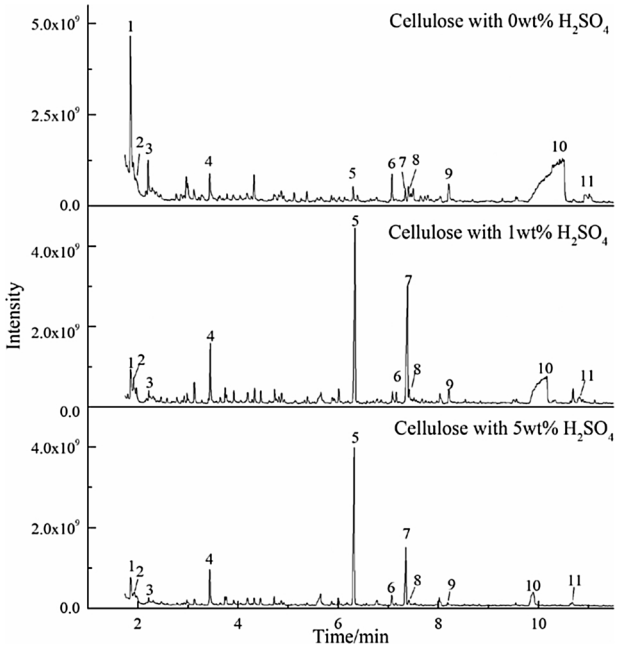

Fig. 4. Typical ion chromatograms from non-catalytic and H_2SO_4-catalyzed fast pyrolysis of cellulose.
(1) HAA (hydroxyacetaldehyde); (2) AA (acetic acid); (3) HA (hydroxyacetone); (4) FF; (5) LGO; (6) LAC (1-hydroxy-3,6-dioxabicyclo[3.2.1]octan-2-one); (7) DGP; (8) 5-HMF (5-hydroxymethyl-furfural); (9) APP (5-anhydro-4-deoxy-D-glycero-hex-1-en-3-ulose); (10) LG; (11) AGF (1,6-anhydro-β-D-glucofuranose).

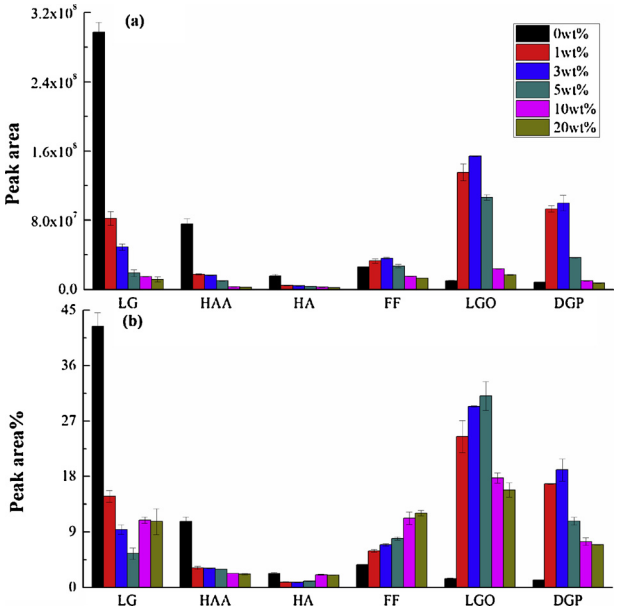

Fig. 5. Peak area and peak area % values of the main products from cellulose with different H_2SO_4 contents.

dehydrated products, and none of these products were predominate in non-catalytic pyrolysis process of cellulose [36,37]. The pyrolytic product distribution altered dramatically in the presence of H_2SO_4. The depolymerized products (i.e., LG) decreased significantly, and also the major ring scission products (HAA and HA). On the contrary, several dehydrated products, i.e., FF, LGO and DGP, increased greatly and became the dominant products in the catalytic process.

Although the analytical Py-GC/MS experiments could not give the quantitative results, it was able to recognize the changes of products yields and concentrations in the pyrolytic vapors under different pyrolytic conditions by comparing the peak area and peak area% values [38,39]. The total peak area values of all detected pyrolytic products are shown in the Supplementary Material (Fig. S1). Fig. S1 shows the continuous decrease of the total peak area value along with the H_2SO_4 content, indicating the monotonous decline of the organic bio-oil yield [11]. The peak area and peak area% values of the main products are shown in Fig. 5, with detailed information of the pyrolytic products shown in the Supplementary Material (Table S1). According to Fig. 5(a), the yields (based on the peak area values) of the typical dehydrated products (FF, LGO and DGP) increased first and then deceased along with the rising of H_2SO_4 content. Especially, the yields of LGO and DGP increased by 14.2 and 10.7 times at 3 wt% of H_2SO_4 content. Whereas, the yields of the depolymerized product and the typical ring scission products all decreased in the presence of H_2SO_4. In addition, according to Fig. 5(b), the presence of H_2SO_4 also significantly altered the relative concentrations (based on the peak area% values) of the pyrolytic products. With the increasing of the H_2SO_4 content, the concentration of FF increased monotonously, while those of LGO and DGP increased first and then decreased. The maximal peak area% values for FF, LGO and DGP reached as high as 12.0% (20.0 wt% H_2SO_4 content), 31.1% (5.0 wt% H_2SO_4 content) and 19.1% (3.0 wt% H_2SO_4 content), respectively. In addition, the concentrations of LG and HA decreased first and then increased, while that of HAA decreased continuously. The peak area% value of LG was as high as 42.3% in the non-catalytic process, but decreased to 14.8% and lower under all catalytic conditions. The peak area% value of HAA also decreased from 10.7% in the non-catalytic process to 3.2% or lower in the catalytic process. Based on above results, it is able to conclude that catalytic pyrolysis of cellulose by H_2SO_4 can significantly increase the yields of typical dehydrated products at the expense of depolymerized and ring scission products.

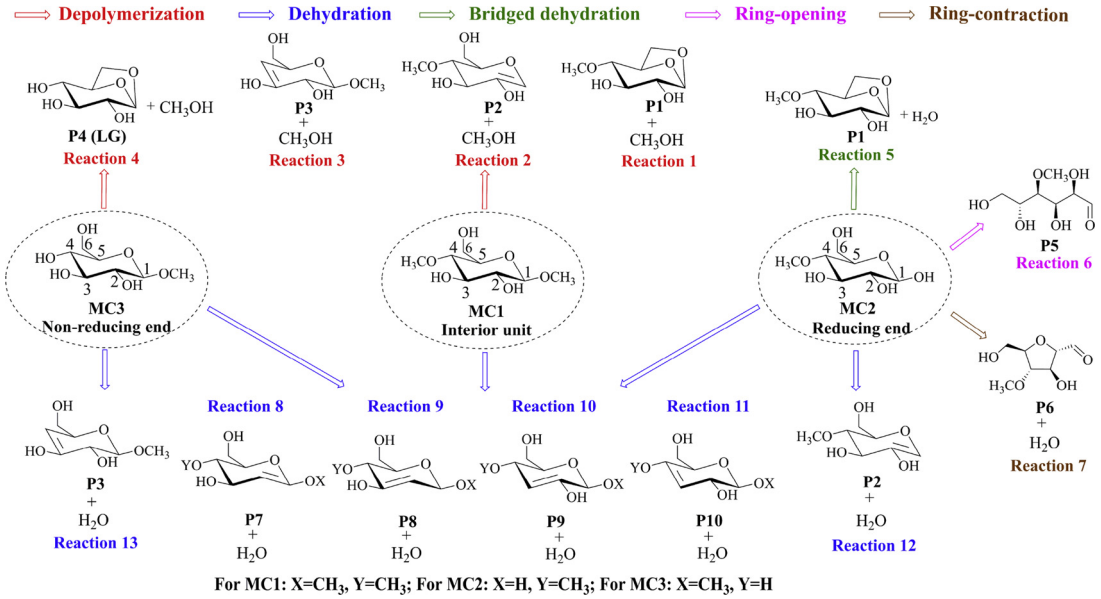

Fig. 6. Major pyrolytic reactions of the interior unit, reducing end and non-reducing end during initial pyrolysis process of cellulose.

3.2. Computational results

3.2.1. Establishment of the H_2SO_4-catalyzed reaction models

As stated in Section 2.2.2, a cellulose chain contains many interior units, a reducing end and a non-reducing end. These basic units will undergo different pyrolytic reactions [31,33,37]. As shown in Fig. 6, in the initial stage of cellulose pyrolysis, the reactions mainly include depolymerization (Reactions 1, 2 and 4 via C1-O1 bond scission; Reaction 3 via C4-O4 bond scission), bridged dehydration (Reaction 5), ring-opening (Reaction 6) ring-contraction (Reaction 7) and dehydration of free hydroxyl groups (Reactions 8–11). Among above basic pyrolysis reactions, depolymerization is the typical initial reaction for both the interior units and the non-reducing end. Whereas, bridged dehydration, ring-opening and ring-contraction are the featured initial pyrolytic reactions for the reducing end. All the three basic units can undergo dehydration of the free hydroxyl groups. Moreover, both reducing end and non-reducing end can undergo additional dehydration (Reactions 12 and 13) due to the hydroxyl groups at C1 and C4 positions, which are similar to the dehydration of the free hydroxyl groups (Reactions 8–11).

The presence of H_2SO_4 can significantly affect the initial pyrolytic reactions of cellulose, and thus changing the following reactions as well as pyrolysis characteristics and product distribution. Due to the strong acidity of H_2SO_4 and the polarity of the hydroxyl groups in cellulose matrix, H_2SO_4 will mainly influence the hydrogen bonds system and the reactions involving hydroxyl groups [6,11]. Based on this fact, H_2SO_4-assisted reaction models were established to investigate the catalytic effect of H_2SO_4 on major initial pyrolytic reactions of cellulose chain, as shown in Fig. 7. **MC1** was employed to investigate the H_2SO_4-assisted depolymerization via C1-O1 bond scission and C4-O4 bond scission in Section 3.2.2. **MC2** was applied to study the H_2SO_4-assisted bridged dehydration, ring-opening and ring-contraction in Section 3.2.3. **MC1**, **MC2** and **MC3** were all used to explore the H_2SO_4-assisted dehydration of free hydroxyl groups in Section 3.2.4. It is noted that **MC3** was not employed to investigate the H_2SO_4-assisted depolymerization, because **MC3** cannot simulate the depolymerization via C4-O4 bond scission.

According to the H_2SO_4-assisted reaction models shown in Fig. 7, the H_2SO_4-assisted depolymerization via C1-O1 bond scission and bridged dehydration take place through a two-step mechanism. On the other hand, other H_2SO_4-assisted reactions occur through a one-step mechanism. In the two-step mechanism, a sulfate ester intermediate is formed by linking the sulfonic group to C1 in the first step. Then H_2SO_4 is recovered with a new H grabbed from 6−OH of the sulfate ester intermediate in the second step. In the one-step mechanism, two types of mechanisms, i.e., “Type A” mechanism and “Type B” mechanism are involved, distinguished by the groups of H_2SO_4 participating in the reactions. In “Type A” mechanism, only one hydroxyl group participates in the reactions, which is similar to the water-assisted or the alcohols-assisted reactions reported in the literature [40–42]. H_2SO_4 exchanges a hydrogen atom with the reactant during the process. Whereas, both hydroxyl and sulfonic groups are involved in “Type B” mechanism. One indigenous S−O bond turns into unsaturated S=O bond, correspondingly another indigenous S=O bond turns into S−O bond. It is notable that only one H_2SO_4-assited dehydration of the free hydroxyl groups is shown in Fig. 7 for a concise illustration, because all the dehydration reactions are almost the same.

3.2.2. Effect of H_2SO_4 on depolymerization of cellulose chain

The adjacent glucose units in cellulose are linked with each other through β-1,4-glucosidic bonds. The breakage of glucosidic bonds (C1-O1 bond and C4-O4 bond) results in the depolymerization of cellulose chain in pyrolysis process. As indicated above, depolymerization is the typical reaction of the interior unit and the non-reducing end. Since the amount of interior units in cellulose chain is much more than that of the non-reducing end, **MC1** (the interior unit) is used to investigate the H_2SO_4-assisted breakage of C1-O1 glucosidic bond and C4-O4 glucosidic bond through both structural and kinetic analyses.

3.2.2.1. Depolymerization via C1-O1 glucosidic bond scission. According to Fig. 6, C1-O1 bond can break through transglycosylation (Reaction 1) and hydrogen shift (Reaction 2) in the non-catalytic process [33,43]. The two reactions result in the formation of a LG end (**P1**) or an unsaturated chain end with C1 = C2 bond (**P2**), respectively. Whereas, in the H_2SO_4-catalyzed process, the C1-O1 bond will break through two successive reactions (Reactions S1 and S2) involving the formation of a sulfate ester intermediate SI1 (Fig. 7). In Reaction S1, CH_3OH (hydroxyl H deriving from H_2SO_4) departs from **MC1** by breaking C1-O1 bond and forms new C1-$O1_{(s)}$ bond, resulting in the formation of sulfate ester intermediate SI1. For SI1, it further evolves into LG end with a new sulfuric acid molecule formed in Reaction S2. The structures of the transition sates STS1 and STS2 in Fig. 8(a) clearly indicate the formation and evolution of the sulfate ester intermediate SI1 in the two-step mechanism. Westmoreland et al. [40] reported similar transition states in the investigation of LG formation from glucose in

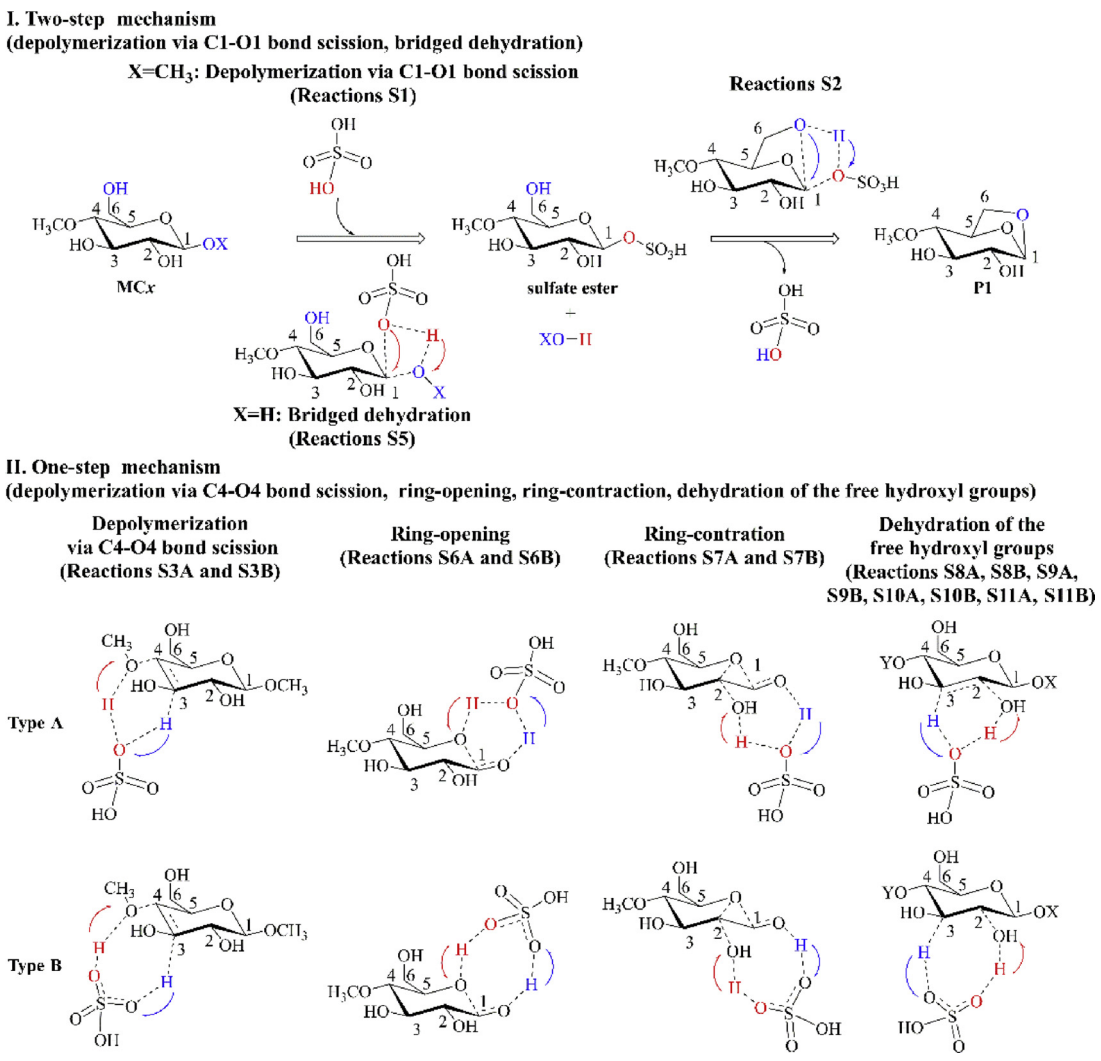

Fig. 7. H_2SO_4-assisted reaction models for major pyrolytic reactions during initial pyrolysis process of cellulose.

the presence of inorganic Brønsted acids. However, their work include only the activation enthalpies (298.15 K) of the formation and evolution of the sulfate ester, without any structural or detailed kinetic information.

To give an insight into the structural changes of **MC1** in the presence of H_2SO_4 in Reactions S1 and S2, the variations of the Mayer bond orders for the formation and evolution of sulfate ester SI1 along IRC coordinates were analyzed, as shown in Fig. 9. In Reaction S1, the bond orders of C1-O1 and $O1_{(s)}$-$H1_{(s)}$ bonds decrease to zero along with the IRC coordinate, and those of C1-$O1_{(s)}$ and O1-$H1_{(s)}$ bonds increase to 0.7 and 0.9, respectively. The variations of bond orders imply the formation of the sulfate ester intermediate SI1. In Reaction S2, the C1-$O1_{(s)}$ bond and O6-H16 bond crack with the formation of C1-O6 bond and $O1_{(s)}$-H16 bond, with corresponding variations of the Mayer bond orders shown in Fig. 9. In addition, C1-$O1_{(s)}$ bond rarely generates in transition sate STS1, whereas, it disappears in transition sate STS2, which suggests that sulfate ester intermediate SI1 is not stable and is readily to decompose. It is consistent with the fact that the gibbs free energy of the sum of SIl and methanol is 20.6 kJ/mol (500 °C), higher than that of the sum of **MC1** and H_2SO_4.

3.2.2.2. Depolymerization via C4-O4 glucosidic bond scission. The C4-O4 glucosidic bond can break through hydrogen shift (Reaction 3 in Fig. 6) during the non-catalytic pyrolysis process. In the catalytic process, C4-

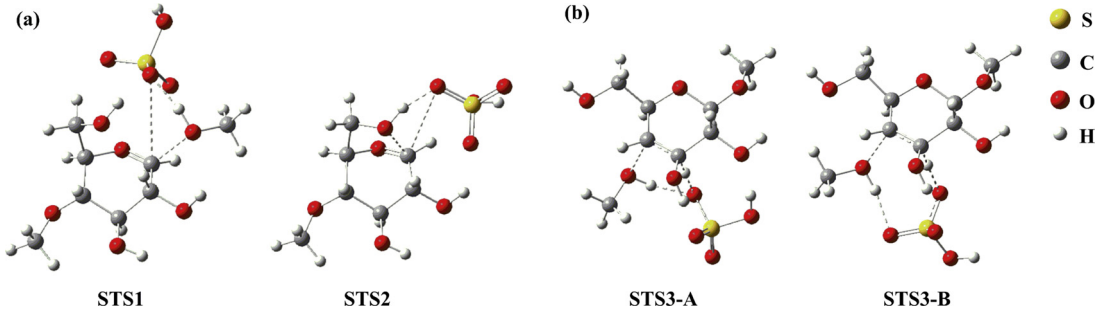

Fig. 8. H_2SO_4-assisted depolymerization via C1-O1 bond scission (a) and via C4-O4 bond scission (b).

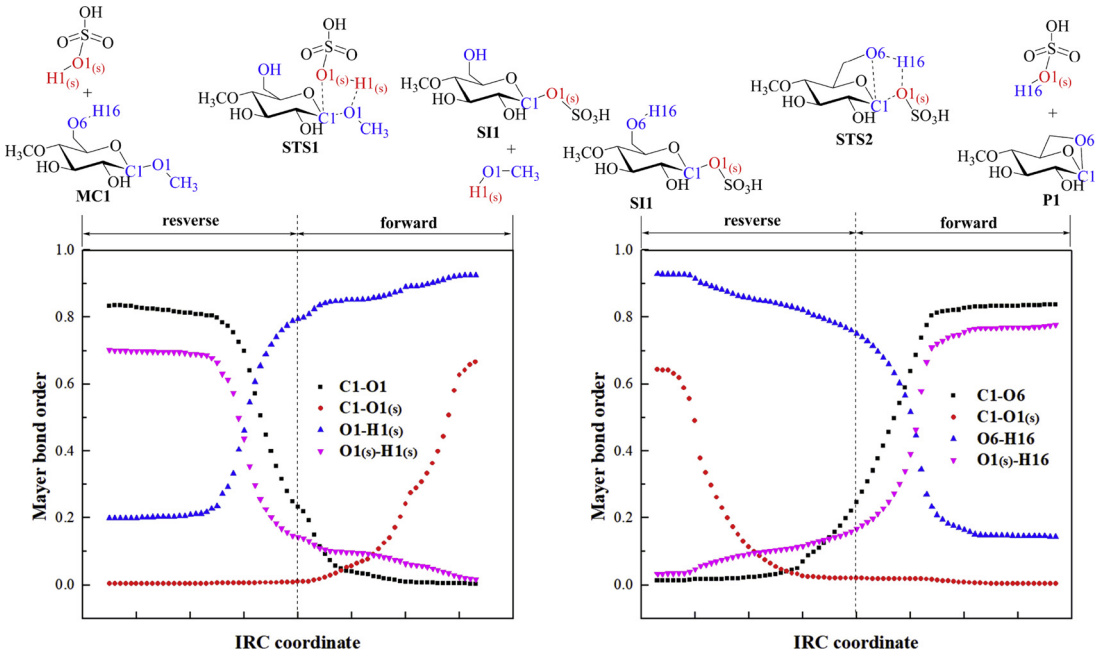

Fig. 9. Variations of the structures and Mayer bond orders along the IRC coordinates for the formation of LG end (P1) over H_2SO_4.

O4 bond will break through H_2SO_4-assisted hydrogen shift without the formation of sulfate ester, which is different from the breakage of C1-O1 glucosidic bond (Fig. 8(a)). In the presence of H_2SO_4, C4-O4 bond may crack via Reaction S3A (with Type A mechanism) and/or Reaction S3B (with Type B mechanism) (Fig. 7), with the structures of the transition states (STS3-A and STS3-B) shown in Fig. 8(b). In Reaction S3A, H_2SO_4 donates $H1_{(s)}$ to O4 and attracts H3 to $O1_{(s)}$ simultaneously. Differently, in Reaction S3B, H_2SO_4 donates $H1_{(s)}$ to O4 and attracts H3 to $O3_{(s)}$ at the meantime, which will result in the formation of the new S = $O1_{(s)}$ and S-$O3_{(s)}$ bonds.

Mayer bond orders along the IRC coordinates were also analyzed for Reaction S3A and S3B, as shown in Fig. 10. In Reaction S3A, the bond order of C4-O4 bond decreases from 0.9 to zero and that of O4-$H1_{(s)}$ bond increases from zero to 0.8 accordingly, implying the formation of CH_3OH (hydroxyl H deriving from H_2SO_4). According to the bond orders of $O1_{(s)}$-$H1_{(s)}$ and $O1_{(s)}$-H3 bonds, H_2SO_4 donates proton to **MC1** first and then acquires another proton form **MC1**. In Reaction S3B, the decrease of $O1_{(s)}$-$H1_{(s)}$ bond order and the increase of O4-$H1_{(s)}$ bond order imply the formation of CH_3OH (hydroxyl H deriving from H_2SO_4). However, the new $O3_{(s)}$-H3 bond will not be formed when CH_3OH has already been generated, as indicated by the bond orders of $O3_{(s)}$-H3 bond and C3-H3 bond. Therefore, it is concluded that when the transfer of the proton from H_2SO_4 to O4 is almost completed, the recovery of H_2SO_4 is still on the scene during the reaction process of Reactions S3A and S3B. It reflects the acidity and the proton donating characteristic of H_2SO_4. In addition, the bond order of S-$O1_{(s)}$ shows a

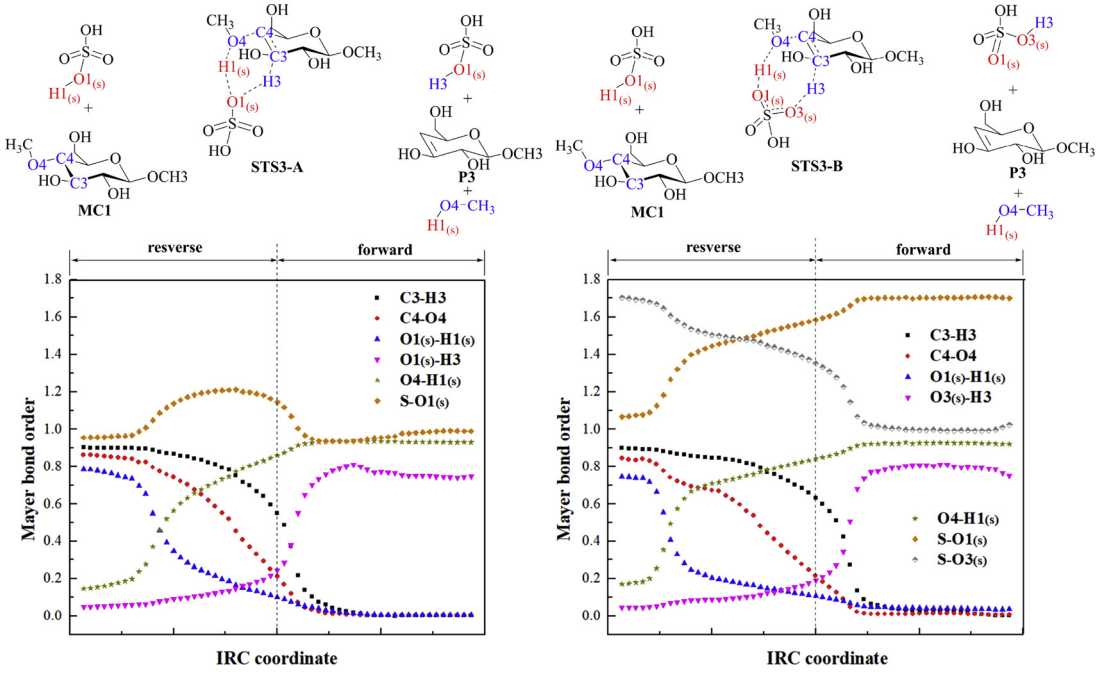

Fig. 10. Variations of Mayer bond orders along the IRC coordinates for C4-O4 bond scission over H_2SO_4.

Table 1
Kinetic parameters for depolymerization reactions.

Without H_2SO_4	$k_{500°C}$ (/s)	A (/s)	E_a (kJ/mol)	H_2SO_4 assisted	$k_{500°C}$ (cm^3/mol/s)	A (cm^3/mol/s)	E_a (kJ/mol)
Reaction 1	3.1E-04	8.9E+13	258.2	Reaction S1	1.1E-18	6.2E-14	65.2
Reaction 2	1.3E-06	5.5E+15	319.6	Reaction S2[a]	3.8E+06	3.0E+12	87.3
Reaction 3	4.3E-07	2.3E+15	321.3	Reaction S3A	2.3E-24	1.1E-13	158.0
				Reaction S3B	4.3E-24	2.1E-12	172.9

[a] The unit is /s for both $k_{500°C}$ and A of Reaction S2 because it is an unimolecular reaction.

trend of first increasing and then decreasing in Reaction S3A, because the new $O1_{(s)}$-H3 bond does not form until $O1_{(s)}$-$H_{(s)}$ bond breaks. On the other hand, the S-$O1_{(s)}$ bond turns into unsaturated S = $O1_{(s)}$ bond, and the unsaturated S = $O3_{(s)}$ bond extends into S-$O3_{(s)}$ bond in Reaction S3B. The different variation tendencies of Mayer bond orders for S-$O1_{(s)}$ and S-$O3_{(s)}$ bonds are attributed to the involvement of only hydroxyl group in Reaction S3A and the involvement of both hydroxyl and sulfonic groups in Reaction S3B.

Following above structural analyses, kinetic analyses were further conducted to determine the kinetic parameters of the reactions for C1-O1 and C4-O4 bonds scission, and the results are shown in Table 1. The activation energies decrease remarkably with the assist of H_2SO_4, implying that H_2SO_4 accelerates the depolymerization reactions by cracking both C1-O1 bond (to form the LG end (1,6-acetal bond) and the non-reducing end) and C4-O4 bond (to form the reducing end). Notably, C1-O1 bond is easier to crack than C4-O4 bond despite the assistance of H_2SO_4, due to the lower activation energies and higher rate constants.

3.2.3. Effect of H_2SO_4 on bridged dehydration, ring-opening and ring-contraction

The bridged dehydration, ring-opening and ring-contraction reactions are typical reactions of the reducing end which is a highly reactive site in cellulose pyrolysis process. Hence, **MC2** (the reducing end) was used to investigate these reactions catalyzed by H_2SO_4. The structures of the transition states in these reactions are shown in Fig. 11.

The bridged dehydration of the reducing end is similar to the transglycosylation of the interior unit. Under non-catalytic conditions, **MC2** undergoes the bridged dehydration through Reaction 5 (Fig. 6). According to Fig. 7, the H_2SO_4-assisted bridged dehydration occurs through two steps of successive reactions (Reactions S5 and S2), also involves the formation of the sulfate ester intermediate SI1, which is similar to the H_2SO_4-assisted depolymerization via C1-O1 bond scission. The detailed information of Mayer bond order analyses for the H_2SO_4-assisted bridged dehydration is indicated in the Supplementary Material (Fig. S2).

According to Fig. 6, during the non-catalytic process, the ring-opening reaction takes place to convert the cyclic structure to the acyclic structure (Reaction 6), and the ring-contraction reaction occurs, resulting in the transformation from the six-membered pyran ring into the five-membered furan ring (Reaction 7). Calculation results imply that both the H_2SO_4-assisted ring-opening and ring-contraction reactions take place through “Type A” (Reactions S6A, S7A) and/or “Type B” (Reaction S6B, S7B) mechanisms, as shown in Fig. 7. According to the Mayer bond order analyses in the Supplementary Material (Figs. S3 and S4), the donating of proton from H_2SO_4 is ahead of the recovery of H_2SO_4, which is similar to the Mayer bond order analyses for Reaction S3A and S3B.

As expected, the kinetic analyses indicate that H_2SO_4 also decreases the activation energies of the three evolution reactions (Table 2). “Type B” reaction paths are more competitive than those of “Type A” for the H_2SO_4-assisted ring-opening and ring-contraction reactions. In both non-catalytic and catalytic processes, ring-opening is the most favorable reaction for the reducing end. In addition, the bridged dehydration is also easy to take place for the reducing end, due to the relatively low activation energy and high rate constant.

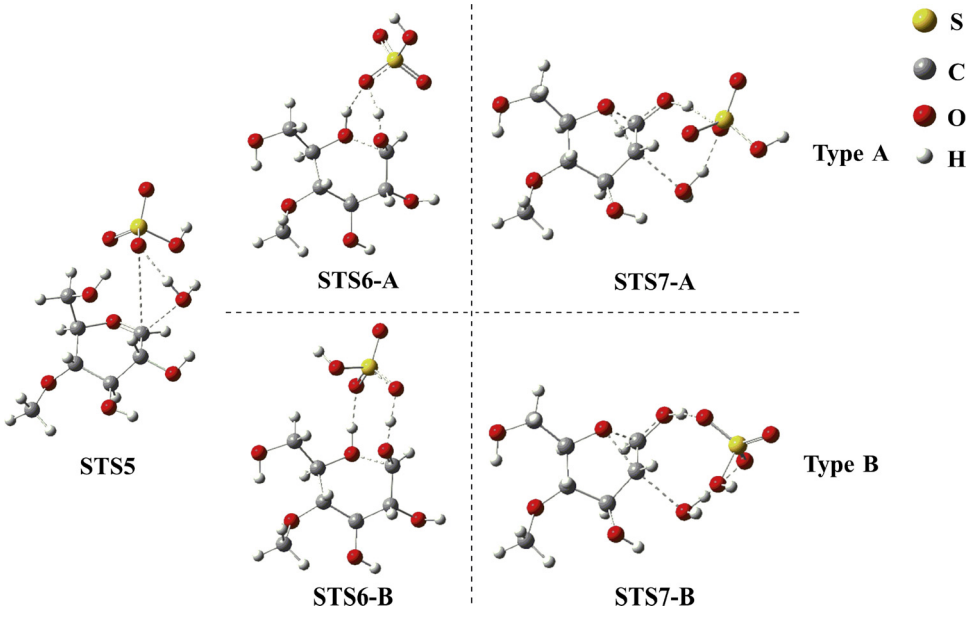

Fig. 11. Structures of the transition states for the H_2SO_4-assisted bridged dehydration, ring-opening and ring-contraction.

Table 2
Kinetic parameters for the bridged dehydration, ring-opening and ring-contraction.

Without H_2SO_4	$k_{500°C}$ (s^{-1})	A (s^{-1})	E_a (kJ/mol)	H_2SO_4 assisted	$k_{500°C}$ ($cm^3/mol/s^{-1}$)	A ($cm^3/mol/s^{-1}$)	E_a (kJ/mol)
Reaction 5	7.6E-04	3.8E+13	247.0	Reaction S5	8.2E-19	9.3E-14	74.6
Reaction 6	2.8E-01	3.2E+13	207.8	Reaction S6A	4.0E-18	1.1E-13	65.4
				Reaction S6B	1.6E-15	1.0E-13	26.4
Reaction 7	7.6E-08	8.6E+13	311.4	Reaction S7A	2.0E-23	2.8E-13	149.8
				Reaction S7B	3.3E-23	2.7E-13	146.4

3.2.4. *Effect of H_2SO_4 on dehydration of free hydroxyl groups*

There are two free hydroxyl groups at C2 and C3 positions (2−OH and 3−OH) on the pyran ring of the cellulose interior unit. Besides the two free hydroxyl groups, the reducing end and non-reducing end have additional free hydroxyl groups at C1 position (1−OH) and C4 position (4−OH), respectively. Dehydration of the free hydroxyl groups are important pyrolytic reactions, which results in the formation of unsaturated C=C bonds. All three basic units of cellulose can undergo dehydration of the free hydroxyl groups. Hence, **MC1**, **MC2** and **MC3** were all used to reveal the influence of H_2SO_4 on these dehydration reactions through structural and kinetic analyses. Compared with the interior unit, the reducing and non-reducing ends undergo additional dehydration of 1−OH (**MC2**) and 4−OH (**MC3**), which shows different dehydration characteristics of the three basic units.

In the non-catalytic process, **MC1** undergoes dehydration reactions through four-membered transition states in Reactions 8–11 (Fig. 6). The H_2SO_4-assisted dehydration reactions take place through six- or eight-membered transition sates in Reactions S8A, S8B, S9A, S9B, S10 A, S10B, S11 A and S11B, which are in similar patterns to the H_2SO_4-assisted C4-O4 bond scission. The structures of these transition states are shown in Fig. 12. The variations of the Mayer bond orders along with the IRC coordinates for these catalytic dehydration reactions are similar to the H_2SO_4-assisted depolymerization via C4-O4 bond scission, thus the detailed information of Mayer bond order analyses for these dehydration reactions is just as that indicated in the Supplementary Material (Figs. S5-S8). Similarly, **MC2** and **MC3** can also dehydrate at these sites (2−OH +1 H/3-H, 3−OH + 2-H/4-H), with the structures of the transition states shown in the Supplementary Material (Fig. S9). Besides the dehydration reactions, **MC2** can also dehydrate at 1−OH + 2-H site under the non-catalytic process. However, this dehydration reaction can hardly happen in the presence of H_2SO_4, due to the intensive reactivity of 1−OH with H_2SO_4 to form the sulfate ester SI1. In regard to **MC3**, it can undergo additional dehydration at 4−OH + 3-H site despite the presence of H_2SO_4. This distinction clearly manifests the different dehydration reactions, resulting from different structural characteristics.

Results of kinetic analysis of the dehydration reactions are almost the same for **MC1**, **MC2** and **MC3**. Hence, Table 3 only shows the kinetic parameters of these dehydration reactions of **MC1**, and the detailed information of the dehydration reactions of **MC2** and **MC3** are given in the Supplementary Material (Table S2). It can be seen that H_2SO_4 decreases the activation energies of dehydration dramatically as compared with the non-catalytic process (152.2–237.7 kJ/mol vs 322.7–327.1 kJ/mol). Hence, dehydration reactions will become very important in H_2SO_4-catalyzed process, which makes the formation of unsaturated structures much easier than in the non-catalytic process. In addition, “Type B” reaction paths are slightly more feasible than “Type A” reaction paths. Activation energies and rate constants are close for dehydration reactions at 2−OH + 3-H, 3−OH + 2-H and 3−OH + 4-H sites. Whereas, dehydration at 2−OH + 1-H site is not as favorable as the other three dehydration reactions despite the assistance of H_2SO_4. As implied in Section 3.2.2, the LG end is readily to be formed with the assistance of H_2SO_4. Hence, H_2SO_4-assisted dehydration reactions of the LG end were also investigated and consistent results were obtained, with the detailed information shown in the Supplementary Material (Fig. S10, Table S3).

3.3. *Discussion on the catalytic mechanism of H_2SO_4 in cellulose pyrolytic reactions*

Based on the calculation results, with the assistance of H_2SO_4 the activation energies of all major reactions decrease during the initial cellulose pyrolysis process, i.e., depolymerization, bridged dehydration, ring-opening, ring-contraction and dehydration. It implies that less energy or lower temperature is required to decompose the H_2SO_4 impregnated cellulose than untreated cellulose. This is consistent with the

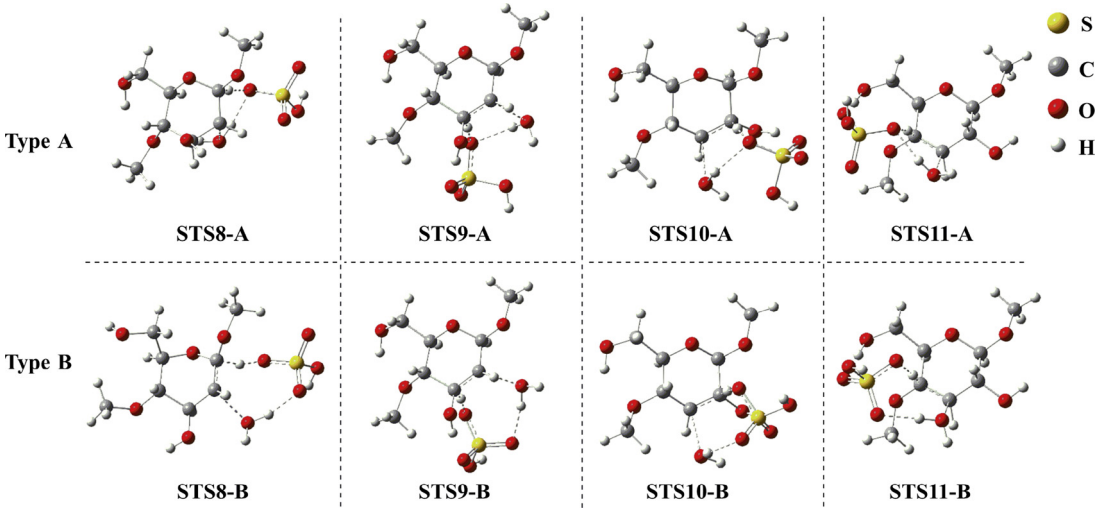

Fig. 12. Structures of the transition states for the H_2SO_4-assisted **MC1** dehydration reactions.

Table 3
Kinetic parameters for dehydration reactions of the **MC1.**

Without H_2SO_4	$k_{500°C}$ (s^{-1})	A (s^{-1})	E_a (kJ/mol)	H_2SO_4 assisted	$k_{500°C}$ ($cm^3/mol/s^{-1}$)	A ($cm^3/mol/s^{-1}$)	E_a (kJ/mol)
Reaction 8	5.3E-11	7.7E+14	372.1	Reaction S8A	5.8E-29	7.0E-13	237.7
				Reaction S8B	5.9E-27	1.6E-12	213.2
Reaction 9	3.4E-08	5.5E+14	328.4	Reaction S9A	3.9E-24	5.6E-13	164.8
				Reaction S9B	1.1E-23	4.4E-13	156.3
Reaction 10	5.6E-08	3.7E+14	322.7	Reaction S10A	1.7E-23	6.1E-13	155.8
				Reaction S10B	7.4E-23	1.5E-12	152.2
Reaction 11	2.5E-08	4.5E+14	329.1	Reaction S11A	9.3E-25	5.3E-13	173.6
				Reaction S11B	1.9E-24	5.5E-13	169.2

TG result that T_{onset} and T_{max} shift to the low temperature region in the presence of H_2SO_4 (Fig. 3). In addition, the promotion of dehydration reactions result in the formation of unsaturated C=C bonds, which will turn into char through crosslinking reactions. As a result, char yield increases in the catalytic pyrolysis process (from 7.5 wt% to 20.5 wt% or higher).

Compared with the non-catalytic pyrolysis process, the types of pyrolytic products are almost identical and no new products are formed in the catalytic process. However, the yields and concentrations of the products altered significantly. To be brief, H_2SO_4 promotes the formation of certain dehydrated products (FF, LGO and DGP) at the expense of the depolymerized product (LG) and the typical ring scission products (HAA and HA). For non-catalytic process, according to Tables 1–3, depolymerization via transglycosylation (Reaction 1) is the most favorable reaction due to the low activation energy (258.2 kJ/mol, Table 1) and the predominance of the interior units in cellulose chain. Hence, the depolymerized product, i.e., LG, is the most abundant organic product in untreated cellulose pyrolysis. In addition, the bridged dehydration of the reducing ends (Reaction 5) is also readily to occur with relatively low activation energy (247.0 kJ/mol, Table 2), contributing to the formation of LG, although the amount of the reducing ends is small in cellulose chain. Ring-opening of the reducing ends (Reaction 6) is another favorable reaction with relatively low activation energy (207.8 kJ/mol, Table 2), following which the ring scission products, especially HAA, are easily formed through the retro-aldol reaction and other reactions. Hence, these ring scission products are very important pyrolytic products. On the contrary, dehydration reactions of the free hydroxyl groups (Reactions 8–11) are relatively difficult to occur because of the high activation energies (322.7–372.1 kJ/mol, Table 3), resulting in relatively low yields of the dehydrated products. Whereas, the competitiveness of the pyrolytic reactions is altered in the presence of H_2SO_4. All major initial reactions are accelerated with the decreased activation energies under the H_2SO_4-catalyzed condition, as shown in Tables 1–3. The depolymerization via C1-O1 bond scission (Reaction S1), the bridged dehydration (Reaction S5) and the ring-opening (Reactions S6A and S6B) still have the lowest activation energies (65.2 kJ/mol, 74.6 kJ/mol, 65.4 kJ/mol, 26.4 kJ/mol, Tables 1 and 2) under catalytic conditions. In particular, the activation energies of the dehydration reactions of the free hydroxyl groups decrease dramatically by using H_2SO_4 (152.2–237.7 kJ/mol, Table 3), implying that the original inconspicuous dehydration reaction in the non-catalytic process becomes very important in the H_2SO_4-catalyzed process. The significantly promoted dehydration reactions play a vital role in changing the yields and concentrations of pyrolytic products. Consequently, several typical products are discussed as follows, to illustrate the changes caused by H_2SO_4 catalysis and to explain the reasons for those changes with the computational results.

In the first place, the yield of the depolymerized product (LG) decreases dramatically in the presence of H_2SO_4 (Fig. 5). According to Broido and co-workers, acid catalysts would catalyze the decomposition of LG [44], which means the secondary decomposition of LG is essential for the decrease of LG yield. Whereas, analytical Py-GC/MS instrument is a very powerful tool to achieve fast pyrolysis of biomass and inhibit the secondary cracking reactions due to the very short vapor residence time in the pyrolysis tube. Once the primary pyrolytic products are formed, they quickly leave the reaction zone with the carrier gas (helium), and thus, avoiding secondary cracking reactions. Based on this fact, it is able to deduce that the decreased LG yield in the H_2SO_4-catalyzed pyrolysis process should not be mainly ascribed to its secondary decomposition, which can be further justified by our computational results. The catalytic effect of H_2SO_4 is mainly responsible for the inhibited formation of LG. During untreated cellulose pyrolysis, LG will be formed when the non-reducing end and the LG end depart from the cellulose chain by depolymerization [33,34]. Both the LG end and the non-reducing end can derive from the depolymerization (transglycosylation) of the interior unit of the cellulose chain. Under the H_2SO_4-catalyzed condition, the decreased yield of LG does not results from the inhibition of the depolymerization. Actually, depolymerization reaction rate is accelerated by H_2SO_4, as discussed in Section 3.2.2. It is the significantly promoted dehydration that converts cellulose into unsaturated structure which can no longer generate LG. As a result, the formation of LG is inhibited, due to the significant decrease of LG precursors in the catalytic process.

Secondly, the yields of typical ring scission products (HAA and HA) also show a decay tendency in the presence of H_2SO_4 (Fig. 5). The ring-opening reaction is accelerated by H_2SO_4. However, the acyclic structure will be unsaturated due to the promoted dehydration of free hydroxyl groups. The unsaturated acyclic structures are not favorable for the occurrence of the retro-aldol reaction which involves the hydroxyl group and carbonyl group at *meta* position. Hence, the formation of the typical ring scission products (especially HAA) is inhibited by H_2SO_4, resulting in a decay of yields. On the contrary, the unsaturated acyclic structure is favorable for the formation of FF [37,45].

Thirdly, the yields of typical dehydrated products (FF, LGO and DGP) increase so greatly that they become the predominate products in the catalytic process (Fig. 5). Apparently, the unsaturated structures resulted from the dehydration of cellulose are favorable in generating dehydrated products. Taking LGO for example, it was regarded as the dehydrated product of LG in the pyrolysis process of pure cellulose in some previous studies [46–48], because of the same 1,6-acetal ring in LG and LGO. However, other studies have confirmed that LGO can be generated via first dehydration and then depolymerization of cellulose chain, without involving LG as the precursor [43,49]. The dehydration reaction is significantly promoted in the catalytic process, which facilitates the LGO formation.

It is notable that the present work merely concentrates on the H_2SO_4-assisted major initial pyrolytic reactions in cellulose pyrolysis, i.e., depolymerization of the cellulose chain, bridged dehydration, ring-opening, ring-contraction, and dehydration of the free hydroxyl groups. In fact, the real pyrolysis process is very complex. For example, water which is derived from the H_2SO_4-assisted dehydration reactions may also participate in the pyrolysis reactions. Moreover, following the

initial pyrolysis process, more complex subsequent reactions take place to generate various pyrolytic products, the pathways for the formation of typical dehydrated products (LGO, DGP and FF) and other products are required to be investigated further. The present work provides an initial insight into the catalytic pyrolysis mechanism of cellulose by H_2SO_4. The fundamental experimental and computational results preliminarily confirm the reliability of this research methodology, and provide a foundation for further investigation into detailed catalytic pyrolysis mechanism and pathways of cellulose by other inorganic acids.

4. Conclusions

In this study, quantum chemistry calculation was performed with 1,4-dimethyl-glucsoe, 4-methyl-glucose and 1-methyl-glucose as the cellulose model compounds to investigate the catalytic mechanism of H_2SO on the major reactions in initial cellulose pyrolysis process, i.e., depolymerization of the cellulose chain, bridged dehydration, ring-opening, ring-contraction and dehydration of the free hydroxyl groups. TGA and Py-GC/MS experiments were also conducted as an assistance for verification. The computational and experimental results well sustain each other, with the following conclusions obtained.

(1) The H_2SO_4-assisted depolymerization via C1-O1 bond scission and bridged dehydration take place in similar two-step mechanism, involving the formation of a sulfate ester intermediate. Whereas, other H_2SO_4-assisted reactions follow one-step mechanism, i.e., depolymerization via C4-O4 bond scission, ring-opening, ring-contraction and dehydration of the free hydroxyl groups. The reactions in the one-step mechanism take place in two different patterns, i.e., “Type A” and “Type B”, distinguished by involving only hydroxyl group or both hydroxyl and sulfonic groups of H_2SO_4 in the reactions.
(2) The activation energies of all the initial pyrolysis reactions decrease with the use of H_2SO_4, resulting in the decrease of the onset temperature of degradation and the temperature of maximum weight loss in TGA experiments. Among all catalytic reactions, dehydration reactions are significantly promoted in the H_2SO_4-catalyzed process as compared with the non-catalytic process. The promoted dehydration reactions play vital roles in the increased char yield.
(3) The presence of H_2SO_4 also significantly alters the volatile organic product distribution obtained in Py-GC/MS experiments. Certain dehydrated products (FF, LGO and DGP) increase significantly, while the depolymerized product (LG) and ring scission products (HAA and HA) decrease remarkably. Promoted dehydration of cellulose favors the formation of unsaturated structures to generate certain dehydrated products as the predominant products in the catalytic process. Meanwhile, the formation of the depolymerized and ring scission products is inhibited, due to the significant decrease of precursors in the catalytic process.

Acknowledgments

The authors thank the National Natural Science Foundation of China (51576064, 51676193), National Basic Research Program of China (2015CB251501), Beijing Nova Program (Z171100001117064), Beijing Natural Science Foundation (3172030), Grants from Fok Ying Tung Education Foundation (161051), and Fundamental Research Funds for the Central Universities (2018ZD08, 2018QN057, 2016YQ05) for financial support.

Appendix A. Supplementary data

Supplementary material related to this article can be found, in the online version, at doi:https://doi.org/10.1016/j.jaap.2018.06.007.

References

[1] S. Wang, G. Dai, H. Yang, Z. Luo, Lignocellulosic biomass pyrolysis mechanism: a state-of-the-art review, Prog. Energy Combust. Sci. 62 (2017) 33–68.
[2] G. Yildiz, F. Ronsse, R. van Duren, W. Prins, Challenges in the design and operation of processes for catalytic fast pyrolysis of woody biomass, Renew. Sustain. Energy Rev. 57 (2016) 1596–1610.
[3] L. Faba, E. Díaz, S. Ordóñez, Recent developments on the catalytic technologies for the transformation of biomass into biofuels: a patent survey, Renew. Sustain. Energy Rev. 51 (2015) 273–287.
[4] S. Zhou, D. Mourant, C. Lievens, Y. Wang, C.Z. Li, M. Garcia-Perez, Effect of sulfuric acid concentration on the yield and properties of the bio-oils obtained from the auger and fast pyrolysis of Douglas Fir, Fuel 104 (2013) 536.
[5] B. Pecha, P. Arauzo, M. Garcia-Perez, Impact of combined acid washing and acid impregnation on the pyrolysis of Douglas fir wood, J. Anal. Appl. Pyrolysis 114 (2015) 127–137.
[6] G. Dobele, D. Meier, O. Faix, S. Radtke, G. Rossinskaja, G. Telysheva, Volatile products of catalytic flash pyrolysis of celluloses, J. Anal. Appl. Pyrolysis 58–59 (2001) 453–463.
[7] X. Meng, H. Zhang, C. Liu, R. Xiao, Comparison of acids and sulfates for producing levoglucosan and levoglucosenone by selective catalytic fast pyrolysis of cellulose using Py-GC/MS, Energy Fuel 30 (2016) 8369–8376.
[8] S. Julien, E. Chornet, R.P. Overend, Influence of acid pretreatment (H_2SO_4, HCl, HNO_3) on reaction selectivity in the vacuum pyrolysis of cellulose, J. Anal. Appl. Pyrolysis 27 (1993) 25–43.
[9] K.Y. Kang, D.Y. Kim, Influence of sulfuric acid impregnation on the carbonization of cellulose, J. Korean Phys. Soc. 60 (2012) 1818–1822.
[10] D.Y. Kim, Y. Nishiyama, M. Wada, S. Kuga, High-yield carbonization of cellulose by sulfuric acid impregnation, Cellulose 8 (2001) 29–33.
[11] S. Wang, Y. Liao, Q. Liu, Z. Luo, K. Cen, Experimental study of the influence of acid wash on cellulose pyrolysis, Front. Chem. Eng. China 1 (2007) 35–39.
[12] Z. Wang, S. Zhou, B. Pecha, R.J.M. Westerhof, M. Garcia-Perez, Effect of pyrolysis temperature and sulfuric acid during the fast pyrolysis of cellulose and Douglas fir in an atmospheric pressure wire mesh reactor, Energy Fuel 28 (2014) 5167–5177.
[13] M.R. Nimlos, S.J. Blanksby, X. Qian, M.E. Himmel, D.K. Johnson, Mechanisms of glycerol dehydration, J. Phys. Chem. A 110 (2006) 6145–6156.
[14] M.R. Nimlos, S.J. Blanksby, G.B. Ellison, R.J. Evans, Enhancement of 1,2-dehydration of alcohols by alkali cations and protons: a model for dehydration of carbohydrates, J. Anal. Appl. Pyrolysis 66 (2003) 3–27.
[15] V. Mamleev, S. Bourbigot, M.Le Bras, J. Yvon, The facts and hypotheses relating to the phenomenological model of cellulose pyrolysis, J. Anal. Appl. Pyrolysis 84 (2009) 1–17.
[16] Z.B. Zhang, Q. Lu, X.N. Ye, L.P. Xiao, C.Q. Dong, Y.Q. Liu, Selective production of phenolic-rich bio-oil from catalytic fast pyrolysis of biomass: comparison of K_3PO_4, K_2HPO_4 and KH_2PO_4, Bioresourse 9 (2014) 4050–4062.
[17] M.J. Frisch, G.W. Trucks, H.B. Schlegel, et al., Gaussian 09, Revision D.01, Gaussian, Inc., Wallingford CT, 2013.
[18] A.D. Becke, Density-functional exchange-energy approximation with correct asymptotic behavior, Phys. Rev. A 38 (1988) 3098–3100.
[19] W. Kohn, A.D. Becke, R.G. Parr, Density functional theory of electronic structure, J. Phys. Chem. 100 (1996) 12974–12980.
[20] S. Grimme, J. Antony, S. Ehrlich, H. Krieg, A consistent and accurate ab initio parametrization of density functional dispersion correction (DFT-D) for the 94 elements H-Pu, J. Chem. Phys. 132 (2010) 154104.
[21] M.W. Wong, Vibrational frequency prediction using density functional theory, Chem. Phys. Lett. 256 (1996) 391–399.
[22] C. Gonzalez, H.B. Schlegel, An improved algorithm for reaction path following, J. Chem. Phys. 90 (1989) 2154–2161.
[23] T. Lu, F. Chen, Multiwfn: a multifunctional wavefunction analyzer, J. Comput. Chem. 33 (2012) 580–592.
[24] S. Canneaux, F. Bohr, E. Henon, KiSThelP: a program to predict thermodynamic properties and rate constants from quantum chemistry results, J. Comput. Chem. 35 (2014) 82–93.
[25] H. Eyring, The activated complex and the absolute rate of chemical reactions, Chem. Rev. 17 (1935) 65–77.
[26] E.P. Wigner, Calculation of the Rate of Elementary Association Reactions, Part I: Physical Chemistry. Part II: Solid State Physics, Springer, Berlin, Heidelberg, 1997.
[27] T. Hosoya, Y. Nakao, H. Sato, H. Kawamoto, S. Sakaki, Thermal degradation of methyl β-D-glucoside. A theoretical study of plausible reaction mechanisms, J. Org. Chem. 74 (2009) 6891–6894.
[28] H.B. Mayes, L.J. Broadbelt, Unraveling the reactions that unravel cellulose, J. Phys. Chem. A 116 (2012) 7098–7106.
[29] Y. Nishiyama, P. Langan, H. Chanzy, Crystal structure and hydrogen-bonding system in cellulose Iβ from synchrotron X-ray and neutron fiber diffraction, J. Am. Chem. Soc. 124 (2002) 9074–9082.
[30] H. Yang, R. Yan, H. Chen, D.H. Lee, C. Zheng, Characteristics of hemicellulose, cellulose and lignin pyrolysis, Fuel 86 (2007) 1781–1788.
[31] M.S. Mettler, A.D. Paulsen, D.G. Vlachos, P.J. Dauenhauer, The chain length effect in pyrolysis: bridging the gap between glucose and cellulose, Green Chem. 14 (2012) 1284–1288.
[32] P.R. Patwardhan, J.A. Satrio, R.C. Brown, B.H. Shanks, Product distribution from fast pyrolysis of glucose-based carbohydrates, J. Anal. Appl. Pyrolysis 86 (2009) 323–330.
[33] R. Vinu, L.J. Broadbelt, A mechanistic model of fast pyrolysis of glucose-based carbohydrates to predict bio-oil composition, Energy Environ. Sci. 5 (2012)

9808–9826.
[34] T. Hosoya, S. Sakaki, Levoglucosan formation from crystalline cellulose: importance of a hydrogen bonding network in the reaction, ChemSusChem 6 (2013) 2356–2368.
[35] Q. Lu, H.Y. Tian, B. Hu, X.Y. Jiang, C.Q. Dong, Y.P. Yang, Pyrolysis mechanism of holocellulose-based monosaccharides: the formation of hydroxyacetaldehyde, J. Anal. Appl. Pyrolysis 120 (2016) 15–26.
[36] B. Hu, Q. Lu, X.Y. Jiang, X.C. Dong, M.S. Cui, C.Q. Dong, Y.P. Yang, Insight into the formation of anhydrosugars in glucose pyrolysis: a joint computational and experimental investigation, Energy Fuel 31 (2017) 8291–8299.
[37] B. Hu, Q. Lu, X. Jiang, X. Dong, M. Cui, C. Dong, Y. Yang, Pyrolysis mechanism of glucose and mannose: the formation of 5-hydroxymethyl furfural and furfural, J. Energy Chem. 27 (2017) 486–501.
[38] Q. Lu, C.Q. Dong, X.M. Zhang, H.Y. Tian, Y.P. Yang, X.F. Zhu, Selective fast pyrolysis of biomass impregnated with $ZnCl_2$ to produce furfural: analytical Py-GC/MS study, J. Anal. Appl. Pyrolysis 90 (2011) 204–212.
[39] Q. Lu, Z. Tang, Y. Zhang, X.F. Zhu, Catalytic upgrading of biomass fast pyrolysis vapors with Pd/SBA-15 catalysts, Ind. Eng. Chem. Res. 49 (2010) 2573–2580.
[40] V. Seshadri, P.R. Westmoreland, Roles of hydroxyls in the noncatalytic and catalyzed formation of levoglucosan from glucose, Catal. Today 269 (2016) 110–121.
[41] T.D. Marforio, A. Bottoni, M. Calvaresi, D. Fabbri, P. Giacinto, F. Zerbetto, The reaction pathway of cellulose pyrolysis to a multifunctional chiral building block: the role of water unveiled by a DFT computational investigation, ChemPhysChem 17 (2016) 3948–3953.
[42] V. Seshadri, P.R. Westmoreland, Concerted reactions and mechanism of glucose pyrolysis and implications for cellulose kinetics, J. Phys. Chem. A 116 (2012) 11997–12013.
[43] Q. Lu, Y. Zhang, C.Q. Dong, Y.P. Yang, H.Z. Yu, The mechanism for the formation of levoglucosenone during pyrolysis of β-D-glucopyranose and cellobiose: a density functional theory study, J. Anal. Appl. Pyrolysis 110 (2014) 34–43.
[44] A. Broido, M. Evett, C.C. Hodges, Yield of 1,6-anhydro-3,4-dideoxy-β-D-glycero-hex-3-enopyranos-2-ulose (levoglucosenone) on the acid-catalyzed pyrolysis of cellulose and 1,6-anhydro-β-D-glucopyranose (levoglucosan), Carbohydr. Res. 44 (1975) 267–274.
[45] M. Wang, C. Liu, X. Xu, Q. Li, Theoretical investigation on the carbon sources and orientations of the aldehyde group of furfural in the pyrolysis of glucose, J. Anal. Appl. Pyrolysis 120 (2016) 464–473.
[46] R.S. Assary, L.A. Curtiss, Thermochemistry and raction brriers for the frmation of lvoglucosenone from cllobiose, ChemCatChem 4 (2012) 200–205.
[47] Y.C. Lin, J. Cho, G.A. Tompsett, P.R. Westmoreland, G.W. Huber, Kinetics and mechanism of cellulose pyrolysis, J. Phys. Chem. C 113 (2009) 20097–20107.
[48] S. Wang, X. Guo, T. Liang, Y. Zhou, Z. Luo, Mechanism research on cellulose pyrolysis by Py-GC/MS and subsequent density functional theory studies, Bioresour. Technol. 104 (2012) 722–728.
[49] H. Kawamoto, S. Saito, W. Hatanaka, S. Saka, Catalytic pyrolysis of cellulose in sulfolane with some acidic catalysts, J. Wood Sci. 53 (2006) 127–133.